https://doi.org/10.1016/j.jpcs.2016.06.004

The following publication Hu, Y., Wang, Y., An, Z., Zhang, J., & Yang, H. (2016). The super-hydrophobic IR-reflectivity TiO2 coated hollow glass microspheres synthesized by soft-chemistry method. Journal of Physics and Chemistry of Solids, 98, 43-49 is available at https://doi.org/10.1016/j.jpcs.2016.06.004.

The super-hydrophobic high IR-reflectivity TiO_2 coated hollow glass microspheres synthesized by soft-chemistry method

Hu Yan[a], Wang Yuanhao[b], Zhenguo An[c], Jingjie Zhang[c] and Yang Hongxing[a,*]

[a] *Renewable Energy Research Group (RERG), Department of Building Services Engineering, The Hong Kong Polytechnic University, Hong Kong*

[b] *Faculty of Science and Technology, Technological and Higher Education Institute of Hong Kong, New Territories, Hong Kong*

[c] *Technical Institute of Physics and Chemistry, Chinese Academy of Sciences, Beijing 100190, China*

Abstract

Hollow glass microspheres (HGM) coated by anatase TiO_2 has been treated as an excellent bi-functional heat insulating material which cannot only blocks the heat transfer inside the material but also reflects most of the irradiated IR rays on the surface. However, the surface of such material is easy to be contaminated and thus its IR reflectivity decreased sharply. To overcome this obstacle, in this paper, a novel tri-functional heat insulating coating with self-cleaning property was developed. TBT and PFOTES were first applied and hydrolyzed on HGM and then underwent hydrothermal reaction to synthesis anatase TiO_2. For comparison, the PFOTES/TiO_2 mutual-coated HGM (MCHGM), PFOTES single-coated HGM (F-SCHGM) and TiO_2 single-coated HGM (Ti-SCHGM) were synthesized as well. Through material characterization such as XRD, SEM, EDS, contact angle, IR reflectivity and thermal conductivity, it was found that uniform anatase TiO_2 and PFOTES layers were coated on HGM surface. The MCHGM had bigger contact angle (153°) but smaller sliding angle (16°) than F-SCHGM (contact angle: 141.2°; sliding angle: 67°). In addition, Ti-SCHGM and MCHGM both showed similar IR reflectivity with ca. 5.8% increase compared with original HGM and F-SCHGM. For the thermal conductivity, coefficients of F-SCHGM (0.0479 W/(m·K)) was basically equal to that of the original HGM (0.0475 W/(m·K)). No obvious difference was found between the thermal conductivity coefficients of PFOTES/TiO_2 MCHGM-coated HGM (0.0543 W/(m·K)) and Ti-SCHGM (0.0546

W/(m·K)).

Keywords

TiO_2; HGM; super-hydrophobicity; IR reflectivity; heat insulating.

1. Introduction

Hollow glass microsphere (HGM) is an inorganic material with micron size that ranges from 10 to 100 μm. The perfect spherical morphology with smooth surfaces and hollow structures endow HGM excellent dispersion, high flow ability, low density and superior thermal insulation property. [1-4] Therefore, it is widely used in many areas, such as the aerospace [5], deep-sea exploration [6, 7], hydrogen storage [8, 9] etc. Even though the hollow space in HGM prevents most of the convective heat transfer [10, 11], the visible light and infrared ray can still be absorbed and transferred through radiation, leading to inferior thermal insulation performance. To prevent the radiant heat transfer, one of the effective strategies is to fabricate core/shell structure via coating IR reflecting layers on HGM. Meanwhile, as an important semiconductor, titanium dioxide (TiO_2) has been widely used in many fields such as photo-catalysis [12-13], solar cells, sensor fabrications [14], environmental applications [15] and energy storage [16]. On the other hand, TiO_2 shows quite low emissivity in the visible light and infrared band, [17] which opens an avenue to obtain composite core/shell structure materials with reduced visible and infrared light absorption, e.g. to controllable synthesis TiO_2 layers on HGMs.

However, the outmost coating is easy to be fouled by the inorganic and organic pollutants, which affect the reflectivity of TiO_2 seriously. Then, the light reflecting property reduces gradually. Therefore, if a further super-hydrophobic self-cleaning property is formed on the TiO_2/HGM, most of the contaminants will be prevented from attaching on the surface, and a durable light reflecting performance can be expected.

In this paper, a simple soft-chemistry method was applied to synthesis super-hydrophobic TiO_2 on HGMs. The schematic diagram was shown in Fig. 1. TBT (Tetrabutyl titanate) and PFOTES (1H,1H,2H,2H-perfluorooctyltriethoxysilane) were firstly hydrolyzed and deposited on HGM surface. In this step, TBT was hydrolyzed into $Ti(OH)_4$. Following that, the hydrothermal was processed in order to turn

amorphous $Ti(OH)_4$ to crystalline anatase TiO_2. For comparison, single-coated HGMs with PFOTES and TiO_2 layers were also synthesized, respectively. This work proposed a simple and facile way to endow the HGM multiple functions.

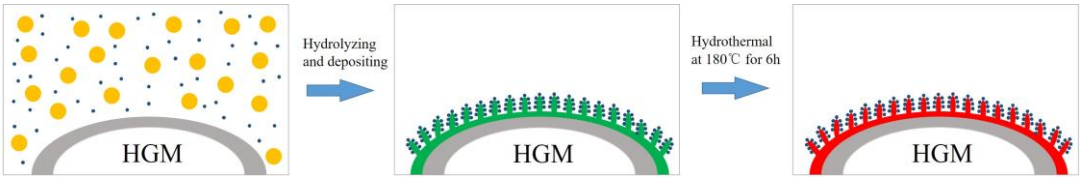

Fig. 1. The schematic of the reaction

●: TBT; ●: PFOTES; ●: $Ti(OH)_4$; ●: Anatase TiO_2

2. Experiments

2.1 Materials

In this work, all the HGM is provided by Technical Institute of Physics and Chemistry, Chinese Academy of Sciences. The particle density of the HGM is 0.3753g/cm^3 and the tap density is 0.2g/cm^3. The wall-thickness of the HGM ranges from 3% to 8% of its diameter. [18] The TBT, PFOTES and ethyl alcohol were bought from Sigma-Aldrich. They were both of analytical grade and do not need further purification.

2.2 Procedures of Experiments

5g HGM, 47.5 ml ethanol and 2.5ml DI water were firstly settled in a three-necked flask with pre-mixing for 20 min by the stirrer in 400 r/min. Next, 15g TBT and 1g PFOTES were mixed in 30 ml ethanol and then dropped into the flask with HGM-ethanol-water mixture by the speed of 1 drop per 7 seconds. The stirrer was kept to running during the dropping. After 3 hours, they were all transferred into a hydrothermal reactor. The reaction lasted for 6 hours in 180 ℃. Subsequently, the samples suspended on the liquid were collected. The final products were obtained after dried in 80 ℃ for 4 hours. Meanwhile, F-SCHGM and Ti-SCHGM were made with same conditions but without TBT and PFOTES, respectively.

3. Characterizations

The X-ray diffraction (XRD) tests were conducted by the Rigaku highly versatile

multipurpose X-ray diffraction system with Cu Kα radiation (λ=0.15406nm) and 2θ ranging from 10° to 80°. The scanning electron microscopy (SEM) images were obtained by the JSM-6490 Scanning Electron Microscope from JEOL. The water contact angle and sliding angle values were obtained by the Contact Angle Goniometer Sindatek Model 100SB from SINDATEK. The reflectivity tests were all processed by the Hitachi U-4100 from Hitachi. The thermal conductivity tests were all characterized by the KYOTO ELECTRONICS QTM-500. The particle size distribution tests were all investigated by Malvern Mastersizer 3000.

4. Results and discussions

4.1 The XRD characterizations

In order to detect if the anatase TiO_2 was successfully formed after the reactions, the XRD tests were processed for characterization. As shown in Fig. 2, the original HGM, F-SCHGM, Ti-SCHGM, MCHGM and standard anatase TiO_2 XRD spectra were displayed, respectively. Since the major component of HGM is amorphous SiO_2 like the glass, only a broad peak at around 2θ=23°were shown in the spectrum of original HGM, which is the characteristic peak of amorphous SiO_2. For the F-SCHGM, its XRD pattern was the same with the original HGM XRD pattern, since the PFOTES did not form a detectable crystal structure and also did not change the HGM lattice. Therefore, only the amorphous SiO_2 broad peak was detected.

For the Ti-SCHGM and MCHGM, as shown in Fig. 2, they were quite alike and a series of peaks at same degrees appeared. Those peaks were able to be steadily indexed to (101), (004), (200), (105), (211), (213) and (204) crystalline planes that correspond to the standard anatase TiO_2 (JCPDS card No. 21-1272) XRD pattern. Because the concentration of TiO_2 in those two samples was not quite high and the background noise cover those signals of TiO_2, some of the characteristic peaks were easily covered and did not occur obviously. In addition, since the HGM can be still detected, the SiO_2 was also detected out by the XRD. Therefore, there were still the broad peaks existing in the XRD pattern of those two samples. However, as explained above, the PFOTES was not able to be detected by XRD and did not change the lattice

of TiO2 or HGM, thus there were no differences between those two samples. Consequently, according to the patterns in Fig. 2, it was confirmed that the anatase TiO_2 was formed in Ti-SCHGM and MCHGM. Since PFOTES could not be detected by XRD and it did not change the lattice of TiO_2 or HGM, there were no differences between the XRD patterns of original HGM and F-SCHGM or Ti-SCHGM and MCHGM.

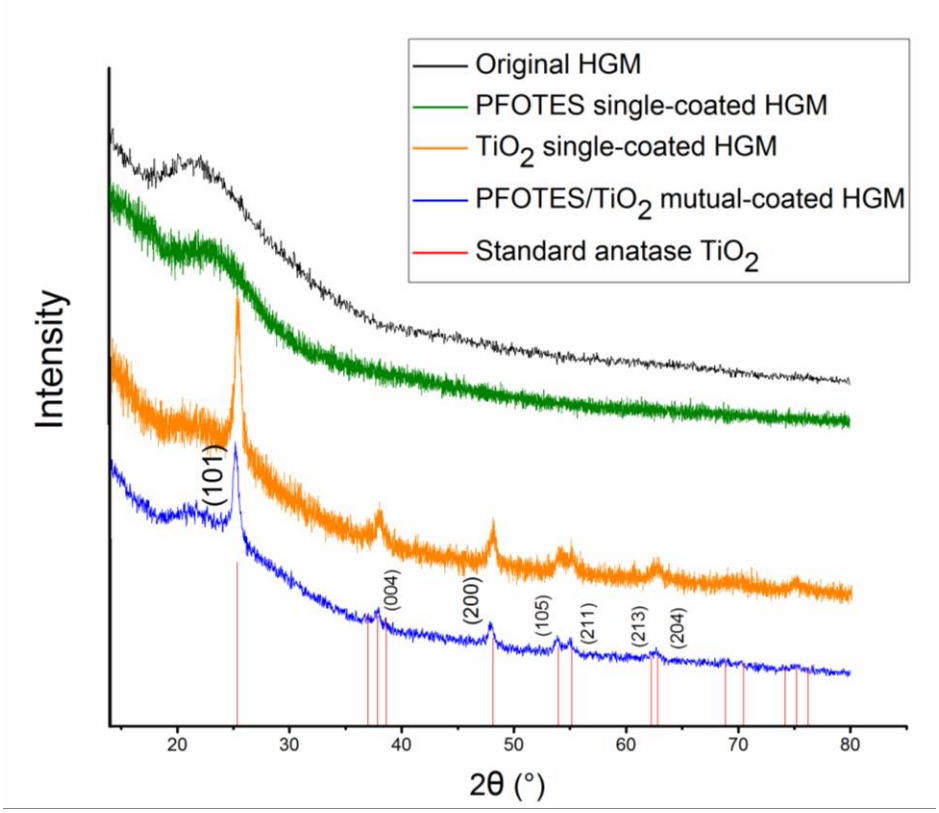

Fig. 2. The XRD spectra of original HGM, super-hydrophobic TiO_2/HGM and standard anatase TiO_2

4.2 The SEM and EDS characterizations

The morphology and the surface elements analysis of those samples above were further detected. The SEM images were shown in Fig. 3. It can be seen that the size of the HGM ranged from 30~50 μm. The original HGM and F-SCHGM displayed a smooth surface while the Ti-SCHGM and MCHGM showed a rough surface coating. For PFOTES, as a kind of silane coupling agent, it was coated on the surface with the thickness of only several molecules. Thus it cannot be detected by SEM. In Fig. 3c and 3d, the coatings were deposited on the HGM and then showed a rougher surface. It derived from the facile reaction conditions. The hydrolysis speed was able to be

adjusted via the drop-wise addition of PFOTES and TBT. Thus the coating was relatively uniform.

As shown in the pink areas of Fig. 3, the EDS was then processed and the results were shown in Fig. 4. In Fig. 4a, it demonstrated the presence of Si, Na, O and Ca, which were the major elements of original HGM. In Fig. 4b, besides the elements revealed above, F was also detected out. Because EDS detected the elements on the surface of selected areas, and F only existed in PFOTES, it was able to determine that PFOTES was coated on HGM surface. for Ti-SCHGM in Fig. 4c, Si, Na, O, Ca and Ti were detected out. Since Ti was the characteristic element of TiO2, and given the XRD patterns above, it was able to conclude that the anatase TiO_2 was deposited on HGM surface. Similarly, in Fig. 4d, F and Ti were simultaneously detected. Thus, both the PFOTES and anatase TiO_2 were on the HGM surface. because of the small amount of F in the reaction, the peak of F was not so strong in Fig. 4b and Fig. 4d.

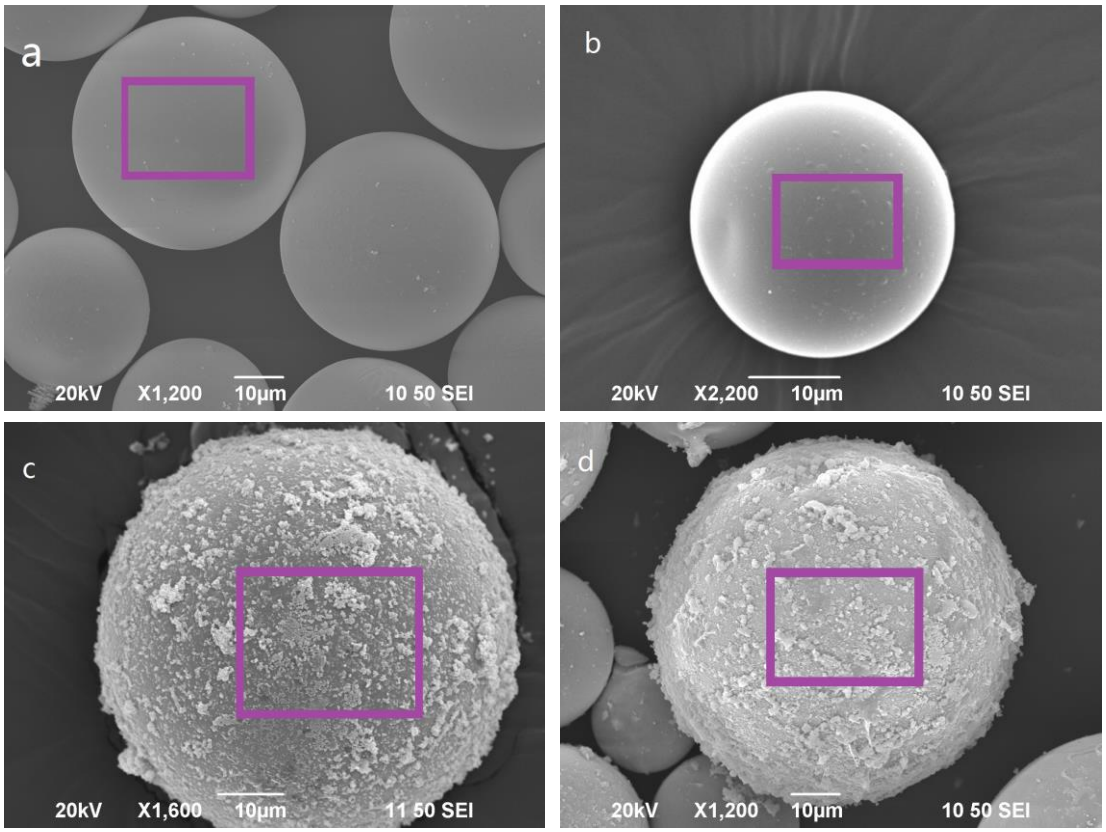

Fig. 3. The morphology of a: original HGM; b: F-SCHGM;
c: Ti-SCHGM; d: MCHGM

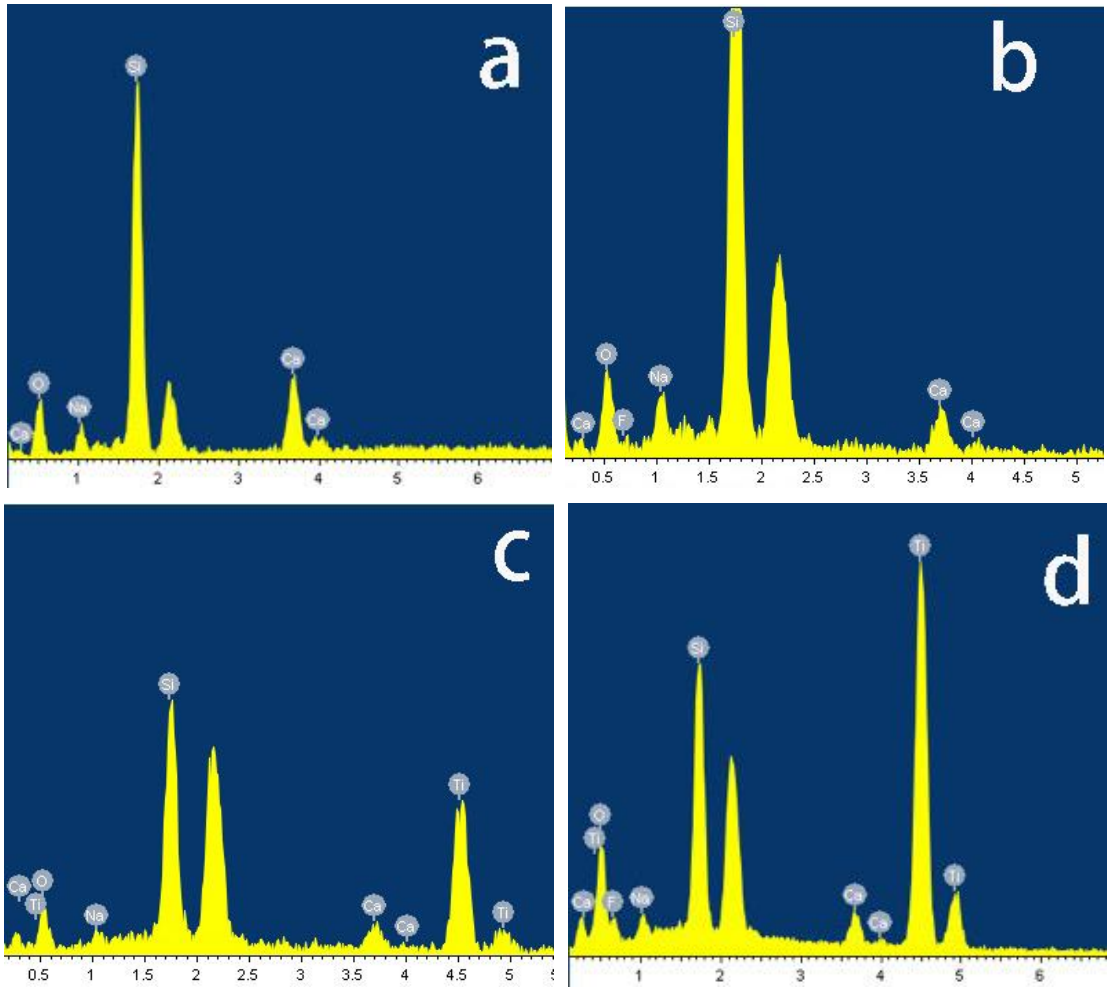

Fig. 4. The EDS measurements of a: original HGM and b: F-SCHGM; c: Ti-SCHGM; d: MCHGM

4.3 The contact angle characterizations

Generally speaking, the water contact angle represents the hydrophilicity or hydrophobicity of a surface. If the contact angle is less than 90°, it is hydrophilicity and in contrary, if more than 90°, it is hydrophobicity. For the super-hydrophilicity and super-hydrophobicity, the contact angles are smaller than 10° and larger than 150° respectively. For the surface which is super-hydrophobic or super-hydrophilic, it is usually considered as self-cleaning surface.

Aiming to detect the hydrophobicity of the TiO_2 coated HGM, the water contact angle values were measured. The results were shown below in Fig. 5. The water contact angle of original HGM (shown in Fig. 5a) was 59°, of F-SCHGM (shown in Fig. 5b) was 141.2°, of Ti-SCHGM (shown in Fig. 5c) was 85° and the MCHGM (shown in Fig. 5d) was 153° whose difference could be distinguished easily since the water drop was

nearly a perfect sphere in Fig. 5b and Fig. 5d. From those two figures, conclusion could be made that PFOTES contributed a lot for the gaining of high contact angle since it was able to decrease the surface energy greatly.

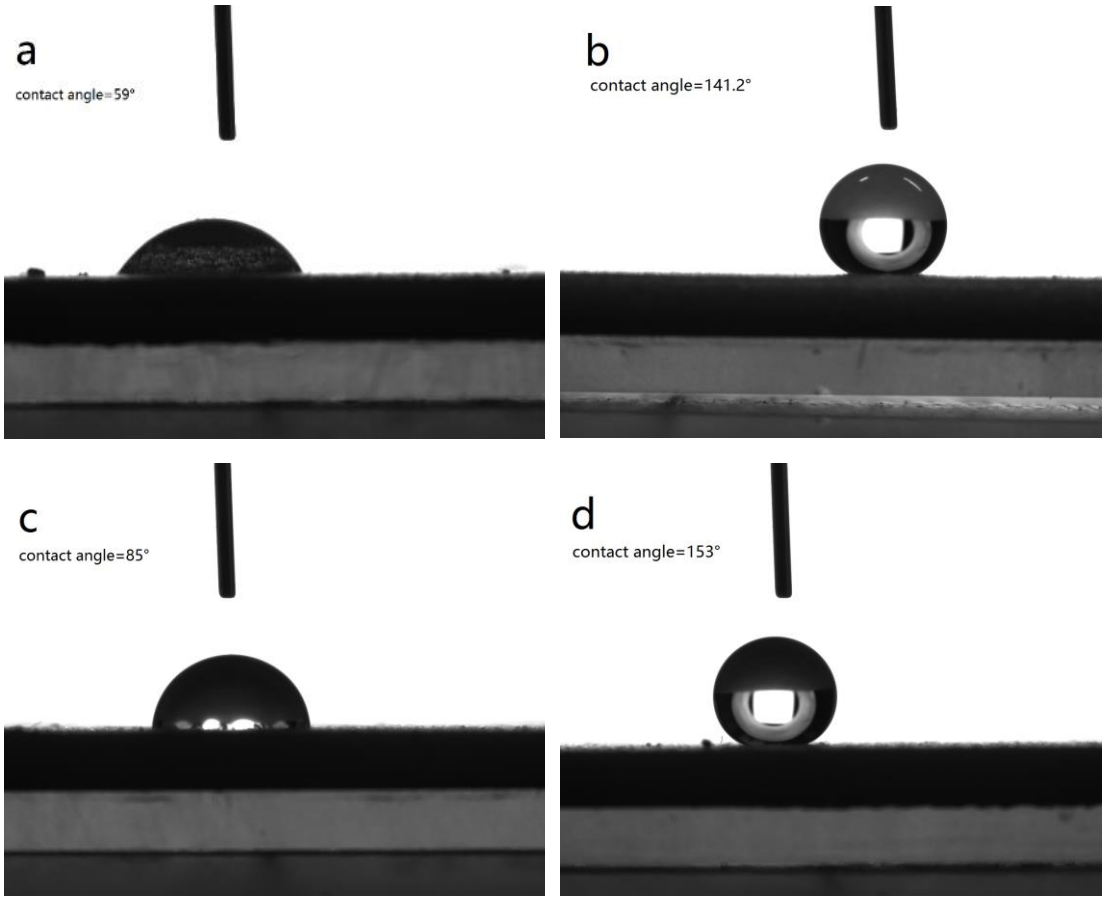

Fig. 5. The contact angle of original HGM (a), F-SCHGM (b), Ti-SCHGM(c) and MCHGM (d)

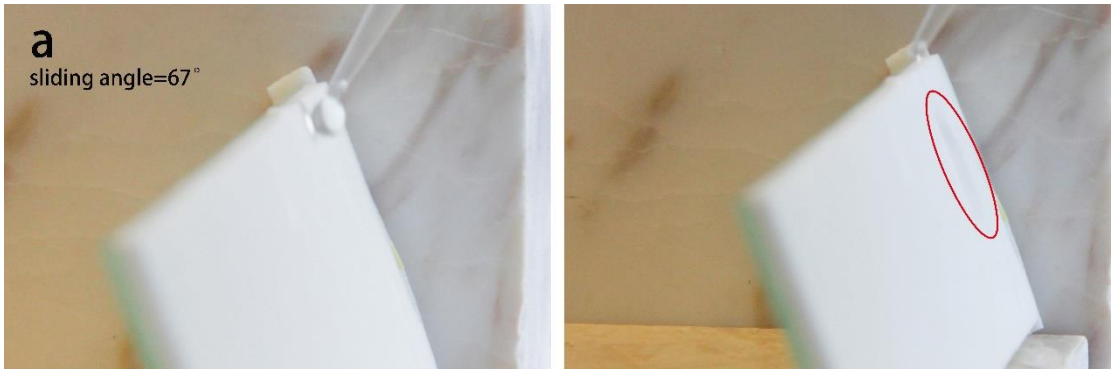

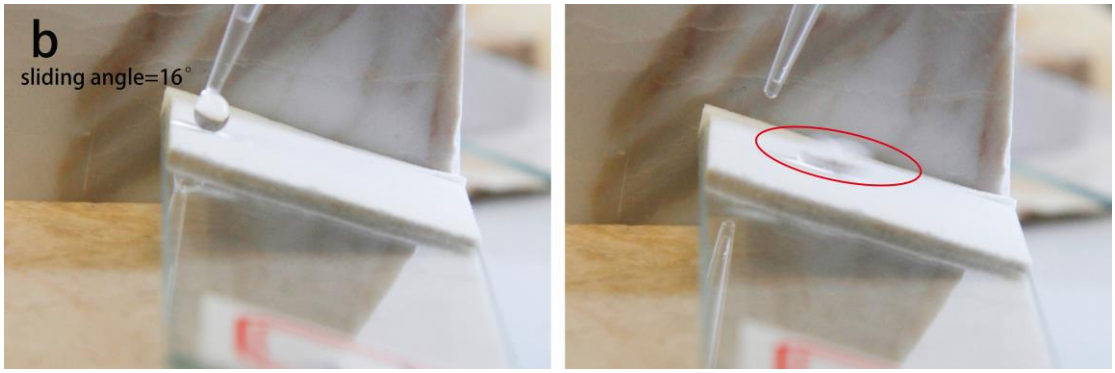

Fig. 6. The sliding angle of F-SCHGM (a) and MCHGM (b)
The red circle marked the sliding path of the water drop.

However, their sliding angle was quite different. The pictures were shown in Fig. 6. As shown in the figure, the sliding angle of F-SCHGM and MCHGM were quite different even though their contact angle were close. According to Cassie-Baxter [19] theory the model was shown in Fig. 7 below. The formula theory was shown in equation (1) [19], where θ^c was the apparent contact angle, θ was Young's contact angle [20], and f was the solid phase fraction. As shown in equation (1), with the decreasing of factor f, the θ^c increased gradually. Therefore, it could be described like in Fig. 7, in which the water drop was supported by a lot of micro solid pillars.

$$\cos\theta^c = f\cos\theta - (1-f) \quad (1)$$

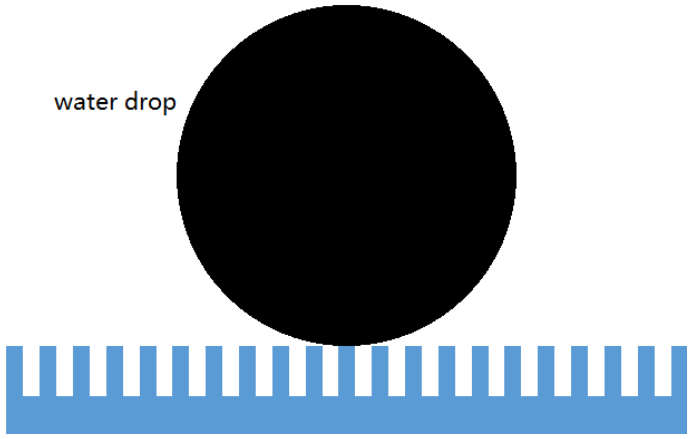

Fig. 7. The Cassie-Baxter wetting theory of super-hydrophobic

Actually, since HGM was in micrometer size, the water drop on the HGM coating surface was not supported by a smooth surface but a non-smooth surface which was made from a lot of micro glass beads. In this case, the factor f of this surface was smaller than an absolute glass surface. According to previous experiments, the contact

angle of a clean smooth glass surface was about 37.9° which was shown in Fig. 8. Contrasted with the original HGM in Fig. 5a with the contact angle of 59°, it was 35% smaller. Therefore, the decrease of factor f increase the contact angle. As for the comparison of original HGM in Fig. 5a and F-SCHGM in Fig. 5b, they had barely same f since the PFOTES coating did not change the surface roughness. However, it decreases the surface energy so drastically that the contact angle increased from 59° to 141.2°. Similarly, as shown in Fig. 5c and Fig. 5d, that is the reason why the contact angle of MCHGM was much bigger than that of Ti-SCHGM. For the comparison of F-SCHGM in Fig. 5b and MCHGM in Fig. 5d, the contact angle in Fig. 5d was slightly higher. The probably reason was still the gaining of roughness, namely the decreasing of factor f, caused by the TiO_2 coating. It can be seen in Fig. 3b and Fig. 3d. Because the contact angle was quite big in Fig. 5b, its gaining derived from the enhancement of roughness was not so obvious. However, their sliding angle still showed big differences, as shown in Fig. 6.

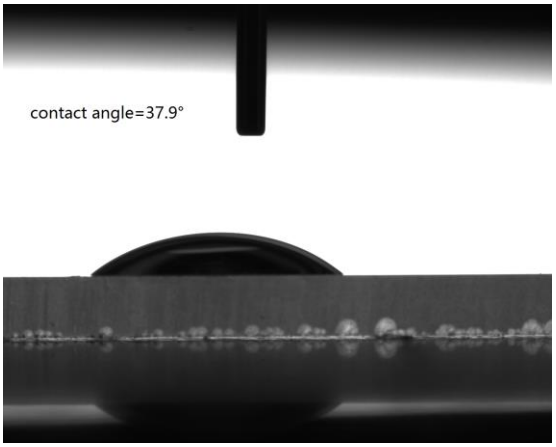

Fig. 8. The water contact angle of a clean smooth glass surface

The picture shown in Fig. 7 was the ideal situation since no water penetrated into the gaps among the pillars because of the surface tension. Practically speaking, the water did penetrate into those gaps more or less. As to the F-SCHGM, the surface roughness was mostly caused by the HGM. Thus the gaps were bigger and then they were easier to be penetrated by water than the MCHGM, which had higher roughness derived from the TiO_2 coating, namely smaller gaps. Following that, the water drop was

half-infiltrated the surface in F-SCHGM while it was much less infiltration in MCHGM. When sliding, the water drop on F-SCHGM endured bigger resistance than on MCHGM. Therefore, the sliding angle differences occurred.

4.4 The reflectivity characterizations

The reflectivity of those samples were characterized and shown below. The main purpose was to detect the reflectivity at IR band, thus the measuring band was from 500 to 2500 nm. As shown in Fig. 9, there were basically two groups of spectra: one was original HGM and F-SCHGM and the other was Ti-SCHGM and MCHGM. The spectra in each group were quite similar. PFOTES hardly change the reflectivity of HGM because firstly, the thickness of the coating was only a few molecules and secondly it did not show a good property of reflectivity. However, the samples with TiO_2 coating showed better reflectivity at IR band (above 750nm). According to this figure, with the help of TiO_2 coating, the reflectivity increased from about 85% to 90%. The increasing range was 5.8%. It was not a big number was because that firstly, the TiO_2 coating was not too thick, which can be solved by adjusting the concentration of TBT and reaction conditions, and secondly, the reflectivity of original HGM was already very high. Therefore, it was demonstrated that with the TiO_2 coating, the IR reflectivity had an obvious decrease.

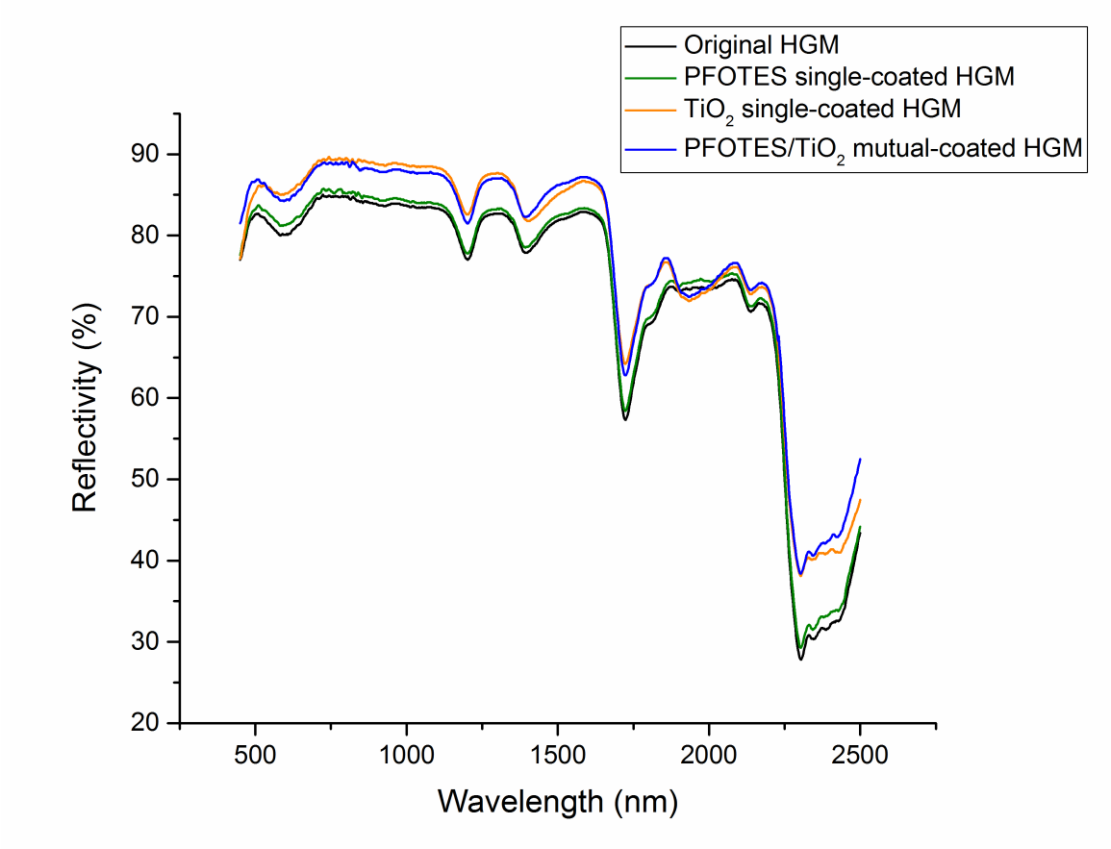

Fig. 9. The reflectivity spectra

4.5 The thermal conductivity characterizations

The thermal conductivity values of those samples were measured in this section. The results were shown in Fig. 10, and their values from sample 1 to 4 were 0.0475 W/(m·K), 0.0479 W/(m·K), 0.0546 W/(m·K) and 0.0543 W/(m·K) respectively. Alike the IR reflectivity data above, the values were divided into two groups: one was the original HGM and F-SCHGM, the other was Ti-SCHGM and MCHGM. The values in each group were quite close. It was because PFOTES, as a coating with a thickness of several molecules, did not change the heat transfer a lot.

However, there were some differences between those two groups, even though the difference was quite small. The formula approximately describing the thermal conductivity of HGM was listed in equation (2) [3], where λ represented the whole thermal conductivity of HGM, λ_s was the thermal conductivity of the solid portion in HGM (namely HGM's wall), φ_s was the volume percentage of the solid portion, λ_g was the thermal conductivity of gas portion and φ_g was the volume percentage of the

gas portion. Since in equation (2), $\lambda_s \gg \lambda_g$ and HGM's wall thickness could be considered as a constant value, λ was closely related to the size of HGM if the major components of HGM remaining unchanged. Therefore, the size distribution was processed and the results was shown in Fig. 11.

$$\lambda \approx \lambda_s \cdot \varphi_s + \lambda_g \cdot \varphi_g \quad (2)$$

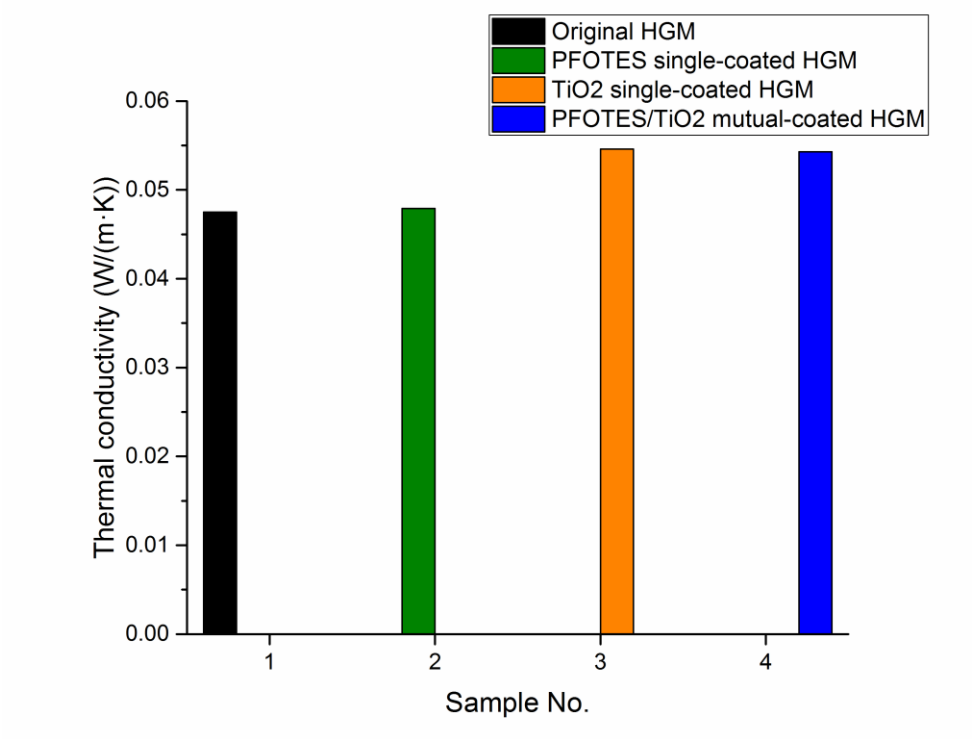

Fig. 10. The thermal conductivity of samples

As shown in Fig. 11, the size distribution of those samples were quite similar. They all ranged from 20-90 μm. Thus, theoretically speaking, they should all have no obvious differences in thermal conductivity. However, actually, the coating of TiO_2 increased the wall thickness of HGM, thus the samples coated with TiO_2 were a little bit higher than the other two. Nevertheless, even though there was a slightly increase of thermal conductivity, the IR reflectivity was enhanced a lot, the whole heat insulation property was enhanced. Also with the help of super-hydrophobic self-cleaning coating, the TiO_2 coating was not polluted easily and the IR reflectivity could remain for a longer time.

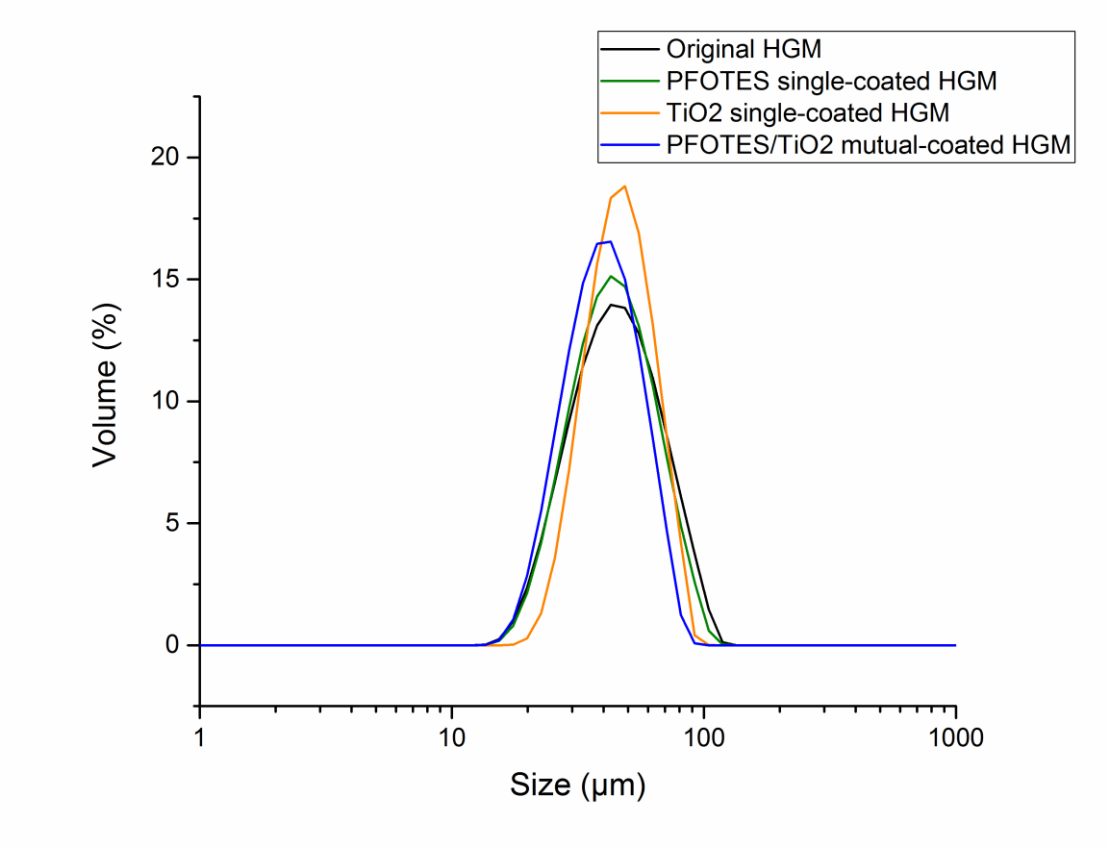

Fig. 11. The size distribution of samples

5. Conclusions

As a summary, in this paper, a super-hydrophobic self-cleaning TiO_2 coated HGM composite material was successfully synthesized via a soft chemistry method. Anatase TiO_2 and PFOTES was demonstrated coated on HGM surface by XRD, SEM and EDS tests and the contact angle values were measured. With the help of TiO_2 coating, the surface roughness was enhanced. Therefore, the contact angle of MCHGM showed higher contact angle value (153°) and lower sliding angle value (141.2°), namely better super-hydrophobicity, than F-SCHGM. In addition, since PFOTES was the coating with the thickness of couple of molecules, it barely changed the IR reflectivity and thermal conductivity of a sample. Consequently, the properties enhancement like that were contributed to the TiO_2. It increased the IR reflectivity for 5.8%. However, since the wall thickness gaining caused by the coating of TiO_2, the thermal conductivity was slightly higher than non-coated ones. Nevertheless, the IR reflectivity was increased, accordingly the whole heat insulation was enhanced. Moreover, with the help of the

super-hydrophobic self-cleaning coating, the HGM was able to work for a longer time by preventing the contamination.

Acknowledgements

The work described in this paper was supported by a grant from the CII-HK / PolyU Innovation Fund. And the great help from Department of Applied Biology & Chemical Technology of The Hong Kong Polytechnic University and The Hong Kong Polytechnic University Research Institute for Sustainable Urban Development (RISUD) is appreciated.

References

[1] Yung K.C., Zhu B.L., Yue T.M., Xie C.S. Preparation and properties of hollow glass microsphere-filled epoxy-matrix composites [J]. Composites Science and Technology, 69 (2): 260-264.

[2] Nan Xu, Jinhui Dai, Zhibin Zhu, Xiang Huang, Pingwei Wu. Synthesis and characterization of hollow glass-ceramics microspheres [J], Composites Science and Technology, 72 (4): 528-532.

[3] Bing Li, JingYuan, Zhenguo An, Jingjie Zhang. Effect of microstructure and physical parameters of hollow glass microsphere on insulation performance [J]. Materials Letters, 65 (12): 1992-1994.

[4] Hu Y, Mei R, An Z, et al. Silicon rubber/hollow glass microsphere composites: Influence of broken hollow glass microsphere on mechanical and thermal insulation property[J]. Composites Science and Technology, 2013, 79: 64-69.

[5] Geleil A.S., Hall M.M., Shelby J.E. Hollow glass microspheres for use in radiation shielding [J]. Journal of Non-Crystalline Solids, 352 (2006) 620–625.

[6] Khimiya, Handbook of Fillers for Polymeric Composite Materials [Russian translation], Moscow (1981).

[7] Greiner-Bar G., "HoNe Mikroglaskugeln. Herstellung, Eigenschaften und Anwendung," Silikattechnik., 40, No. 1, 23-25 (1989).

[8] Kool, “Method for storing hydrogen, and related articles and systems”, United States Patent 7749304, 2010.

[9] Brow Richard K, Schmitt Melodie L. A survey of energy and environmental application of glass[J]. Journal of the European Ceramic Society, 29 (2009) 1193–1201.

[10] Awaja F, Arhatari B D. X-ray Micro Computed Tomography investigation of accelerated thermal degradation of epoxy resin/glass microsphere syntactic foam[J]. Composites Part A: Applied Science and Manufacturing, 2009, 40(8): 1217-1222.

[11] Wang S, Luo R, Ni Y. Preparation and characterization of resin-derived carbon foams reinforced by hollow ceramic microspheres[J]. Materials Science and Engineering: A, 2010, 527(15): 3392-3395.

[12] Carp O, Huisman C L, Reller A. Photoinduced reactivity of titanium dioxide[J]. Progress in solid state chemistry, 2004, 32(1): 33-177.
[13] Fujishima A, Rao T N, Tryk D A. Titanium dioxide photocatalysis[J]. Journal of Photochemistry and Photobiology C: Photochemistry Reviews, 2000, 1(1): 1-21.
[14] Fujishima A. Electrochemical photolysis of water at a semiconductor electrode[J]. Nature, 1972, 238: 37-38.
[15] Hoffmann M R, Martin S T, Choi W, et al. Environmental applications of semiconductor photocatalysis[J]. Chemical reviews, 1995, 95(1): 69-96.
[16] Chen X, Mao S S. Titanium dioxide nanomaterials: synthesis, properties, modifications, and applications[J]. Chemical reviews, 2007, 107(7): 2891-2959.
[17] Yuan J, An Z, Li B, et al. Facile aqueous synthesis and thermal insulating properties of low-density glass/TiO_2 core/shell composite hollow spheres[J]. Particuology, 2012, 10(4): 475-479.
[18] PAN S, ZHANG J, SONG G. Research progress of hollow glass microsphere and solid buoyant material for deep-sea application[J]. Journal of Tropical Oceanography, 2009, 4: 004.
[19] Cassie A B D, Baxter S. Wettability of porous surfaces[J]. Transactions of the Faraday Society, 1944, 40: 546-551.
[20] Wenzel R N. Resistance of solid surfaces to wetting by water[J]. Industrial & Engineering Chemistry, 1936, 28(8): 988-994.